JACS
JOURNAL OF THE AMERICAN CHEMICAL SOCIETY
Communication
pubs.acs.org/JACS

# Superconductivity with Topological Surface State in $Sr_xBi_2Se_3$

Zhongheng Liu,[†,‡] Xiong Yao,[†,‡] Jifeng Shao,[†,‡] Ming Zuo,[‡] Li Pi,[†,‡,§] Shun Tan,[‡] Changjin Zhang,*[,†,‡,§] and Yuheng Zhang[†,‡,§]

[†]High Magnetic Field Laboratory, Chinese Academy of Sciences and University of Science and Technology of China, Hefei 230026, PR China

[‡]Hefei National Laboratory for Physical Sciences at Microscale, University of Science and Technology of China, Hefei 230026, PR China

[§]Collaborative Innovation Center of Advanced Microstructures, Nanjing University, Nanjing 210093, PR China

Supporting Information

**ABSTRACT:** By intercalation of alkaline earth metal Sr in $Bi_2Se_3$, superconductivity with large shielding volume fraction (~91.5% at 0.5 K) has been achieved in $Sr_{0.065}Bi_2Se_3$. Analysis of the Shubnikov–de Hass oscillations confirms the half-shift expected from a Dirac spectrum, giving transport evidence of the existence of surface states. Importantly, $Sr_xBi_2Se_3$superconductor is stable under air, making $Sr_xBi_2Se_3$ an ideal material base for investigating topological superconductivity.

The theoretical prediction and successful experimental realizations of topological insulators have opened an exciting research topic in physics and materials fields.[1−4] These and related materials have attracted much interest not only in investigating their exotic topological properties but also in the search for new topological phases. A particularly exciting new phase is topological superconductivity,[5,6] which features the existence of gapless surface states at the surfaces of a fully gapped superconductor. Because of the unique electronic structure, topological superconductors are believed to have great potential applications in fault-tolerant topological quantum computing.

Despite the importance to both materials science and potential applications, experimental realizations of topological superconductors have been greatly limited. One way to realize possible topological superconductivity is based on the proximity effects at the interface of topological insulator thin films grown on superconducting substrates.[7−9] Besides proximity-induced superconductivity, the realization of possible topological superconductivity in bulk material could be very important, especially in real application. By intercalation of Cu in $Bi_2Se_3$ topological insulator, bulk superconductivity can be achieved in single crystals.[10,11] Recently, tremendous experimental and theoretical efforts have been directed toward this material both to improve the sample quality and to clarify whether or not this and related compounds are really topological superconductors.[12−23] However, no consensus has yet been reached. The divergence is mainly due to the relatively low superconducting volume fraction (~50%) of the $Cu_xBi_2Se_3$ samples.[10,11,21] At present, the experimental realization of bulk topological superconductors remains a big challenge. The answer to this problem greatly relies on the fabrication of an appropriate material with large superconducting volume fraction and the identification of its surface states.

Here we show that intercalation of Sr in the well-known topological insulator $Bi_2Se_3$ could lead to a superconducting state below ~2.5 K. Bulk superconductivity has been confirmed by the large shielding volume fraction (91.5%). The quantum oscillations data measured with magnetic fields up to 35 T give the $-^1/_2$ intercept in the limit $1/B \rightarrow 0$, providing transport evidence of the existence of surface states. Moreover, $Sr_xBi_2Se_3$ samples are stable in air, which is important in real application.

We have grown a series of $Sr_xBi_2Se_3$ samples with nominal Sr content of 0−0.3. The typical dimensions of the obtained single crystals are about $3 \times 3 \times 0.5$ mm$^3$. The resultant crystals are easily cleaved along the basal plane, leaving a silvery shining-mirror-like surface. To determine the chemical compositions of the obtained samples, we perform energy-dispersive X-ray spectroscopy (EDX) analysis of $Sr_xBi_2Se_3$ samples. The EDX spectrum shown in Figure 1a confirms the existence of Sr, Bi, and Se. However, we find that for each sample the real Sr content is less than the nominal content (Table S1). In particular, the real Sr content can be only about 0.065 when the nominal Sr content is $x = 0.19$. For $Bi_{2-x}Sr_xSe_3$ and the actual Sr contents are comparable to the nominal compositions.

Figure 1b shows the powder X-ray diffraction (XRD) patterns of $Bi_2Se_3$, $Sr_{0.062}Bi_2Se_3$, and $Bi_{1.85}Sr_{0.15}Se_3$ samples. Detailed refinements of XRD patterns suggest that the lattice parameters of $Sr_xBi_2Se_3$ are $a = 4.1369$ Å and $c = 28.598$ Å, which are larger than those of undoped $Bi_2Se_3$ ($a = 4.1328$ Å and $c = 28.573$ Å), and the lattice constants of $Bi_{1.85}Sr_{0.15}Se_3$ sample are determined to be $a = 4.146$ Å and $c = 28.559$ Å. It is found that the $c$-axis lattice constant of $Bi_{2-x}Sr_xSe_3$ decreases with increasing Sr-doping content. Thus, the slight increase in the $c$-axis constant in $Sr_{0.062}Bi_2Se_3$ supports the idea that Sr atoms are intercalated in the $Bi_2Se_3$ lattice.

Figure 1c gives the temperature dependence of in-plane resistivity ($\rho_{xx}$ vs $T$ curve) of $Sr_{0.062}Bi_2Se_3$ and $Bi_{1.85}Sr_{0.15}Se_3$ samples. Resistivity of $Sr_{0.062}Bi_2Se_3$ sample exhibits metallic-like behavior at high temperature. Below ~50 K, the $\rho_{xx}$ vs $T$ curve is very flat, giving the residual resistivity $\rho_{xx0} = 0.24$ mΩ cm. The onset of superconducting transition occurs at $T_c \approx 2.57$ K, and zero resistivity is achieved at $T_0 \approx 2.39$ K. For $Bi_{1.85}Sr_{0.15}Se_3$

**Received:** July 1, 2015
**Published:** August 11, 2015





DOI: 10.1021/jacs.5b06815
J. Am. Chem. Soc. 2015, 137, 10512−10515

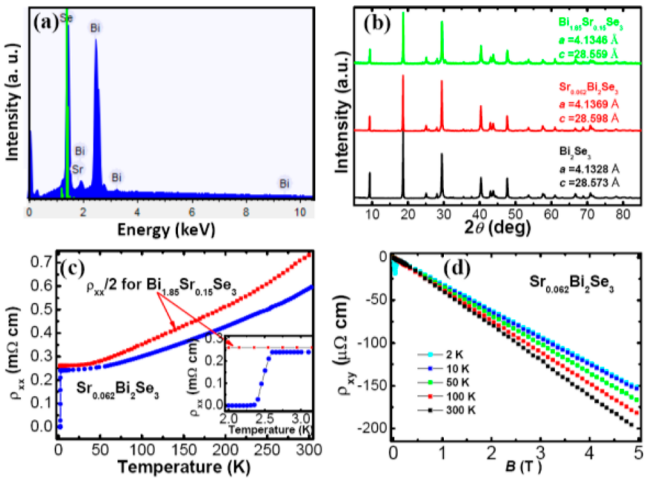


**Figure 1.** (a) Representative energy-dispersive X-ray spectroscopy pattern showing the existence of Sr, Bi, and Se. (b) Powder X-ray diffraction patterns of $Bi_2Se_3$, $Sr_{0.062}Bi_2Se_3$, $Bi_{1.85}Sr_{0.15}Se_3$ samples. (c) Temperature dependence of resistivity of $Sr_{0.062}Bi_2Se_3$ sample and $Bi_{1.85}Sr_{0.15}Se_3$ sample. (d) Magnetic field dependence of transverse resistivity of $Sr_{0.062}Bi_2Se_3$ sample measured at different temperatures.

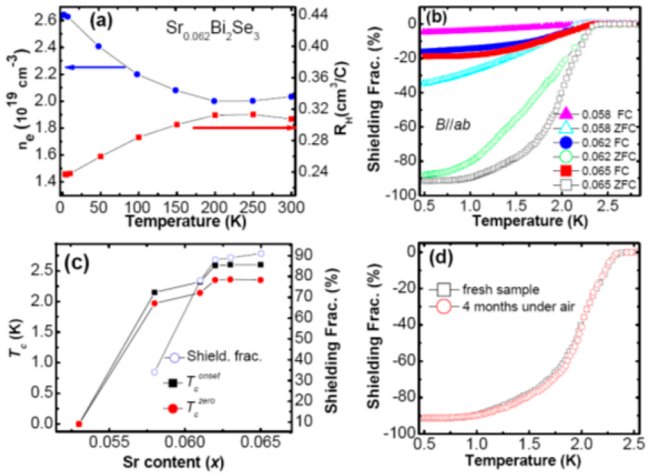


**Figure 2.** (a) Hall coefficient $R_H$ and charge carrier density $n_e$ as estimated from Figure 1d. (b) Temperature dependence of magnetic susceptibility for $Sr_xBi_2Se_3$ samples. (c) Plot of the onset transition temperature ($T_c^{onset}$), zero-resistivity temperature ($T_c^0$), and the shielding fraction at 0.5 K at different Sr content. (d) Comparison between the temperature dependence of magnetic susceptibility of the freshly obtained $Sr_{0.065}Bi_2Se_3$ sample and that exposed under air for 4 months (the same piece).

sample, no superconducting transition has been observed down to 1.9 K, suggesting that Sr-doped $Bi_2Se_3$ samples are not superconducting. (We have confirmed that all $Bi_{2-x}Sr_xSe_3$ samples are not superconducting within $x \leq 0.25$, Figure S6.) To determine the type and density of charge carriers in $Sr_{0.062}Bi_2Se_3$ sample, we perform the measurement of Hall resistivity. Figure 1d shows that the Hall resistivity $\rho_{xy}$ is almost proportional to the applied magnetic field $B$, suggesting the dominance of only one type of bulk carrier. The negative slope of the $\rho_{xx}$ vs $B$ curve means that the dominant charge carriers in $Sr_{0.062}Bi_2Se_3$ are electrons. The Hall coefficient $R_H$ slightly decreases with decreasing temperature, and the carrier concentration ($n_e$) is found to increase from $2.02 \times 10^{19}$ $cm^{-3}$ at 300 K to $2.65 \times 10^{19}$ $cm^{-3}$ below 10 K (Figure 2a). This carrier density is about six times smaller than that of $Cu_xBi_2Se_3$,[11] suggesting that the Fermi level is closer to the Dirac point in the present sample and the carrier mobility in $Sr_{0.062}Bi_2Se$ sample is moderate ($\mu(3\ K) = 1/n_e\rho_{xx}(3\ K)$ e $\approx$ 870 $cm^2/(V\ s)$).

Figure 2b gives the temperature dependence of magnetic susceptibility for $Sr_{0.058}Bi_2Se_3$, $Sr_{0.062}Bi_2Se_3$, and $Sr_{0.065}Bi_2Se_3$ samples. The applied magnetic field is 2 Oe with $B \parallel ab$. In the $B \parallel ab$ case, we ignore the effect of the demagnetization factor because the dimensions of the samples satisfy $a \approx b \gg c$. For $Sr_{0.058}Bi_2Se_3$, diamagnetic signal appears below 2.2 K, indicating the occurrence of bulk superconductivity. The shielding volume fraction of $Sr_{0.058}Bi_2Se_3$ sample is about 34% at 0.5 K. For $Sr_{0.062}Bi_2Se_3$ and $Sr_{0.065}Bi_2Se_3$ samples, diamagnetic signal appears at ~2.35 K. In these samples, a large shielding fraction has been obtained. For example, the shielding fraction at 0.5 K can reach up to 88% in $Sr_{0.062}Bi_2Se_3$. For $Sr_{0.065}Bi_2Se_3$, the shielding fraction can be as high as 91.5% below 1 K. Figure 2c plots the superconducting transition temperature as well as the shielding fraction (at 0.5 K) for $Sr_xBi_2Se_3$ samples. Both the transition temperature and the shielding fraction increase with increasing Sr content when $x \leq 0.065$. We have placed $Sr_xBi_2Se_3$ samples under air for 4 months and found that the superconducting volume fraction does not decrease (Figure 2d) suggesting that the samples are stable. This is in sharp contrast to the behavior of $Cu_xBi_2Se_3$ samples, where the superconductivity is damaged over exposure under air for several hours.

To determine whether or not there is a surface state in $Sr_xBi_2Se_3$ system, we performed quantum oscillation measurements on $Sr_{0.062}Bi_2Se_3$ sample. Figure 3a,c givea the magnetic

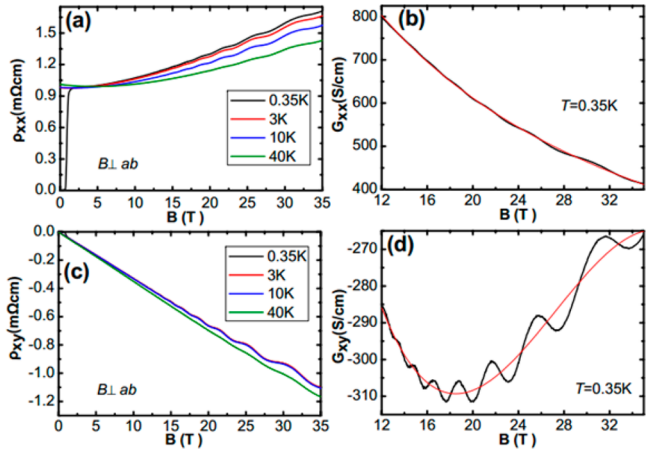


**Figure 3.** (a) Magnetic field dependence of in-plane resistivity at different temperatures with magnetic field perpendicular to the $ab$ plane. (b) Converted in-plane conductance at 0.35 K. (c) Magnetic field dependence of Hall resistivity. (d) Converted Hall conductance at 0.35 K.

field dependence of in-plane resistivity ($\rho_{xx}$) and Hall resistivity ($\rho_{xy}$) of $Sr_{0.062}Bi_2Se_3$ sample measured with $B \perp ab$, respectively. At 0.35 K, the pronounced Shubnikov–de Haas (SdH) oscillation can be observed when the magnetic field is larger than 10 T in both the $\rho_{xx}$ vs $B$ curve and the $\rho_{xy}$ vs $B$ curve. With increasing temperature, the amplitude of the SdH oscillation decreases. When $T > 40$ K, the magnitudes of the SdH oscillations are greatly weakened. From the $\rho_{xy}$ vs $B$ curves in Figure 3c, it is estimated that the electron carrier


DOI: 10.1021/jacs.5b06815
J. Am. Chem. Soc. 2015, 137, 10512–10515

concentration is about $n_e \approx 2.6 \times 10^{19}$ cm$^{-3}$, consistent with that given in Figure 2a.

In bulk $Bi_2Se_3$-type samples, the surface conductance ($G^s$) is usually small comparing to the bulk conductance ($G^b$).[24,25] When the surface conduction channel coexists with the bulk conduction channel, the observed conductance matrix is the sum $G_{xx} = G^s_{xx} + G^b_{xx}$ and $G_{xy} = G^s_{xy} + G^b_{xy}$. In this case, the experimentally measured resistivity and Hall effect are contributed to by both the surface conductance ($G^s_{xx}$ and $G^s_{xy}$) and the bulk conductance ($G^b_{xx}$ and $G^b_{xy}$). Thus, simply from the measured $\rho_{xx}$ vs $B$ curves and the $\rho_{xy}$ vs $B$ curves one cannot determine the Landau index. As has been suggested by Xiong et al.,[25] it is expedient to convert the $\rho_{xx}$ and $\rho_{xy}$ into the conductance $G_{xx} = \rho_{xx}/[\rho_{xx}^2 + \rho_{xy}^2]$ and $G_{xy} = \rho_{xy}/[\rho_{xx}^2 + \rho_{xy}^2]$. In Figure 3b,d, we plot the converted $G_{xx}$ vs $B$ curve and the $G_{xy}$ vs $B$ curve at 0.35 K, respectively. Here we show only the data at 0.35 K because the $G_{xx}$ vs $B$ curves and the $G_{xy}$ vs $B$ curves at other temperatures exhibit the same oscillatory period with the curves at 0.35 K.

Figure 4a shows the SdH oscillation of $\Delta G_{xx}$ against $1/B$ after subtracting the background. The simple oscillatory pattern

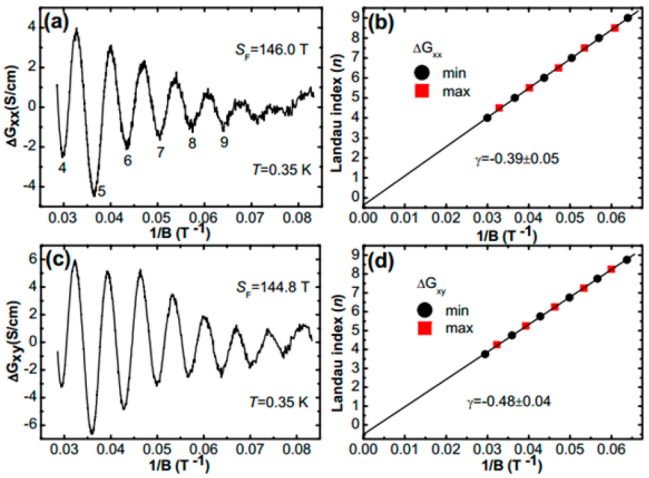


**Figure 4.** (a) Oscillatory component of the in-plane conductance at 0.35 K plotted against $1/B$. The Landau level indices ($n$) = 4, 5, 6, ... are indicated for the minima of $\Delta G_{xx}$. (b) $n$ vs $1/B$, where $n$ and $n + {}^1/_2$ correspond to the minima and maxima of $\Delta G_{xx}$, respectively. (c) Oscillatory component of the Hall conductance at 0.35 K plotted against $1/B$. (d) $n$ vs $1/B$ derived from c, where $1/B$ is plotted against $n + {}^1/_4$. The ${}^1/_4$ shift arises because the minima in $d\Delta G_{xy}/dB$ align with the minima in $\Delta G_{xx}$.[25]

is the result of the single frequency $F$ = 146 T. This frequency is slightly larger than (or comparable to) that of $Bi_2Se_3$,[26,27] whereas it is smaller than that of $Cu_xBi_2Se_3$.[16,17] Figure 4b plots the minima of $\Delta G_{xx}$ (solid circles) and the maxima of $\Delta G_{xx}$ (red squares), which are shifted by ${}^1/_2$. From Figure 4b, one can see that the best-fit straight line intercepts the $n$ axis at the value $\gamma = -0.39 \pm 0.05$. The same analysis is applied to the Hall conductance (Figure 4c). The frequency determined from the $\Delta G_{xy}$ vs $1/B$ curve is $F$ = 144.8 T, in agreement with that determined from the $\Delta G_{xx}$ vs $1/B$ curve. Figure 4d shows the plot based on the minima and maxima of the Hall conductance $\Delta G_{xy}$. The minima in $\Delta G_{xy}$ correspond to $n + {}^1/_4$ because the derivative $d\Delta G_{xy}/dB$ has minima at $n$.[25] The intercept of the fitted line occurs at $\gamma = -0.48 \pm 0.04$. It is found that these intercepts are quite close to the ideal Dirac case $\gamma = -{}^1/_2$ rather than the Schrödinger case where $\gamma = 0$. The slight deviation of $\gamma$ value from $-{}^1/_2$ could be probably due to an additional phase shift resulting from the curvature of the Fermi surface in the third direction, which changes from 0 for a quasi-2D cylindrical Fermi surface to $\pm{}^1/_8$ for a corrugated 3D Fermi surface ($-0.39 \pm 0.05 = -(0.515-1/8) \pm 0.05$).[28] Thus, the high-field SdH oscillation results clearly reveal the existence of a nontrival $\pi$ Berry's phase ($\gamma = {}^1/_2$) and thus provide strong evidence of the existence of Dirac Fermions in $Sr_xBi_2Se_3$. In topological insulators $Bi_2Se_3$ and $Bi_2Te_3$, the gapless Dirac Fermions are accompanied by the surface states. The present SdH oscillation data may provide transport evidence for the existence of surface states in $Sr_xBi_2Se_3$samples. The existence of topological properties in $Sr_xBi_2Se_3$ superconductors could be further confirmed by angle-resolved photoemission spectroscopy and scanning tunneling spectroscopy as well as other experiments.

In conclusion, we have successfully grown a series of high-quality $Sr_xBi_2Se_3$ single-crystal superconductors. The samples exhibit very high shielding volume fraction (91.5%). From the high-field SdH oscillations, we find the transport evidence of the existence of the surface states, probably suggesting that $Sr_xBi_2Se_3$ compounds are topological superconductors. More importantly, $Sr_xBi_2Se_3$ samples are completely insensitive to air. The stability of $Sr_xBi_2Se_3$ samples is very helpful both in future fundamental investigation and in possible electronic applications.

## ■ ASSOCIATED CONTENT

### Supporting Information

The Supporting Information is available free of charge on the ACS Publications website at DOI: 10.1021/jacs.5b06815.

Experimental details, supporting table and figures are included in the Supporting Information. (PDF)

## ■ AUTHOR INFORMATION


### Corresponding Author

*zcjin@ustc.edu.cn


### Author Contributions

Z.L., X.Y., and J.S. contributed equally to this work

### Notes

The authors declare no competing financial interest.

## ■ ACKNOWLEDGMENTS

We acknowledge Xianhui Chen, Zhong Fang, Donglai Feng, and Xingjiang Zhou for helpful discussions. This work was supported by the National Natural Science Foundation of China (Grant Nos. 11174290 and U1232142), and the Scientific Research Grant of Hefei Science Center of Chinese Academy of Sciences (Grant No. 2015SRG-HSC025).

## ■ REFERENCES

(1) Kane, C. L.; Mele, E. J. *Phys. Rev. Lett.* **2005**, *95*, 146802.
(2) Bernevig, B. A.; Hughes, T. L.; Zhang, S. C. *Science* **2006**, *314*, 1757−1761.
(3) Zhang, H. J.; Liu, C. X.; Qi, X. L.; Dai, X.; Fang, Z.; Zhang, S. C. *Nat. Phys.* **2009**, *5*, 438−432.
(4) Kambe, T.; Sakamoto, R.; Kusamoto, T.; Pal, T.; Fukui, N.; Hoshiko, K.; Shimojima, T.; Wang, Z. F.; Hirahara, T.; Ishizaka, K.; et al. *J. Am. Chem. Soc.* **2014**, *136*, 14357−14360.
(5) Qi, X. L.; Hughes, T. L.; Raghu, S.; Zhang, S. C. *Phys. Rev. Lett.* **2009**, *102*, 187001.
(6) Fu, L.; Kane, C. L. *Phys. Rev. Lett.* **2008**, *100*, 096407.



DOI: 10.1021/jacs.5b06815
J. Am. Chem. Soc. 2015, 137, 10512−10515

(7) Wang, M. X.; Liu, C. H.; Xu, J. P.; Yang, F.; Miao, L.; Yao, M. Y.; Gao, C. L.; Shen, C. Y.; Ma, X. C.; Chen, X.; Xu, Z. A.; Liu, Y.; Zhang, S. C.; Qian, D.; Jia, J. F.; Xue, Q. K. *Science* **2012**, *336*, 52−55.
(8) Zareapour, P.; Hayat, A.; Zhao, S. Y. F; Kreshchuk, M.; Jain, A.; Kwok, D. C.; Lee, N.; Cheong, S. W.; Xu, Z. J.; Yang, A.; Gu, G. D.; Jia, S.; Cava, R. J.; Burch, K. S. *Nat. Commun.* **2012**, *3*, 1056.
(9) Xu, J. P.; Wang, M. X.; Liu, Z. L.; Ge, J. F.; Yang, X. J.; Liu, C. H.; Xu, Z. A.; Guan, D. D.; Gao, C. L.; Qian, D.; Liu, Y.; Wang, Q. H.; Zhang, F. C.; Xue, Q. K.; Jia, J. F. *Phys. Rev. Lett.* **2015**, *114*, 017001.
(10) Hor, Y. S.; Williams, A. J.; Checkelsky, J. G.; Roushan, P.; Seo, J.; Xu, Q.; Zandbergen, H. W.; Yazdani, A.; Ong, N. P.; Cava, R. J. *Phys. Rev. Lett.* **2010**, *104*, 057001.
(11) Kriener, M.; Segawa, K.; Ren, Z.; Sasaki, S.; Ando, Y. *Phys. Rev. Lett.* **2011**, *106*, 127004.
(12) Fu, L.; Berg, E. *Phys. Rev. Lett.* **2010**, *105*, 097001.
(13) Wray, L. A.; Xu, S. Y.; Xia, Y. Q.; Hor, Y. S.; Qian, D.; Fedorov, A. V.; Lin, H.; Bansil, A.; Cava, R. J.; Hasan, M. Z. *Nat. Phys.* **2010**, *6*, 855−859.
(14) Wan, X. G.; Savrasov, S. Y. *Nat. Commun.* **2014**, *5*, 4144.
(15) Sasaki, S.; Kriener, M.; Segawa, K.; Yada, K.; Tanaka, Y.; Sato, M.; Ando, Y. *Phys. Rev. Lett.* **2011**, *107*, 217001.
(16) Lawson, B. J.; Hor, Y. S.; Li, L. *Phys. Rev. Lett.* **2012**, *109*, 226406.
(17) Koski, K. J.; Cha, J. J.; Reed, B. W.; Wessells, C. D.; Kong, D. S.; Cui, Y. *J. Am. Chem. Soc.* **2012**, *134*, 7584−7587.
(18) Hsieh, T. H.; Fu, L. *Phys. Rev. Lett.* **2012**, *108*, 107005.
(19) Malliakas, C. D.; Chung, D. Y.; Claus, H.; Kanatzidis, M. G. *J. Am. Chem. Soc.* **2013**, *135*, 14540−14543.
(20) Levy, N.; Zhang, T.; Ha, J.; Sharifi, F.; Talin, A. A.; Kuk, Y.; Stroscio, J. A. *Phys. Rev. Lett.* **2013**, *110*, 117001.
(21) Kriener, M.; Segawa, K.; Sasaki, S.; Ando, Y. *Phys. Rev. B* **2012**, *86*, 180505(R).
(22) Yang, S. A.; Pan, H.; Zhang, F. *Phys. Rev. Lett.* **2014**, *113*, 046401.
(23) Schneeloch, J. A.; Zhong, R. D.; Xu, Z. J.; Gu, G. D.; Tranquada, J. M. *Phys. Rev. B: Condens. Matter Mater. Phys.* **2015**, *91*, 144506.
(24) Qu, D. X.; Hor, Y. S.; Xiong, J.; Cava, R. J.; Ong, N. P. *Science* **2010**, *329*, 821−824.
(25) Xiong, J.; Luo, Y. K.; Khoo, Y.; Jia, S.; Cava, R. J.; Ong, N. P. *Phys. Rev. B: Condens. Matter Mater. Phys.* **2012**, *86*, 045314.
(26) Analytis, J. G.; Chu, J. H.; Chen, Y. L.; Corredor, F.; McDonald, R. D.; Shen, Z. X.; Fisher, L. R. *Phys. Rev. B: Condens. Matter Mater. Phys.* **2010**, *81*, 205407.
(27) Taskin, A. A.; Sasaki, S.; Segawa, K.; Ando, Y. *Adv. Mater.* **2012**, *24*, 5581−5585.
(28) Murakawa, H.; Bahramy, M. S.; Tokunaga, M.; Kohama, Y.; Bell, C.; Kaneko, Y.; Nagaosa, N.; Hwang, H. Y.; Tokura, Y. *Science* **2013**, *342*, 1490−1493.


DOI: 10.1021/jacs.5b06815
*J. Am. Chem. Soc.* 2015, 137, 10512−10515